Optimization and testing of groove-shaped grid-controlled modulated X-ray tube for X-ray communication

Zhaopeng Feng, Yunpeng Liu *, Junxu Mu, Wenxuan Chen, Sheng Lai, Xiaobin Tang **

Department of Nuclear Science and Technology, Nanjing University of Aeronautics and Astronautics, Nanjing 210016, China
Key Laboratory of Nuclear Technology Application and Radiation Protection in Astronautics, Ministry of Industry and Information Technology, Nanjing 210016, China

ARTICLE INFO

ABSTRACT

The current modulated X-ray source for X-ray communication (XCOM) are facing the problems of low bandwidth and weak X-ray intensity. In this paper, a groove-shaped grid-controlled modulated X-ray tube (GGMXT) with hot-cathode was proposed to improve the modulation performance. With cut-off voltage and tube current as objective function, a CST-Matlab co-simulation based on the non-dominated sorting genetic algorithm II (NSGA-II) was developed to optimize the grid structure of GGMXT. The simulation results shows that the cut-off voltage of GGMXT can be controlled between −71 and −3 V with corresponding X-ray intensity of 99.0% to 54.8% of the maximum value. Based on the optimized results, four different prototypes of GGMXT, including three optimized tubes and one non-optimized tube, were prepared, tested, and compared with the simulated version. The effectiveness of the optimization method was demonstrated through testing. Compared with the non-optimized tube, one optimized GGMXT prototype obtains a relatively low cut-off voltage of −5 V@50 kV while maintaining high X-ray emission intensity. Its modulation bandwidth is higher than 3 MHz and the X-ray pulse repetition rate is in excess of several MHz. Therefore, the optimized GGMXT shows excellent modulation signal emission performance and great application potential in the field of X-ray communication.

1. Introduction

X-ray communication (XCOM) uses X-rays as carriers to transmit information based on intensity modulation-direct detection (IM-DD). In 2007, Gendreau of Goddard Flight Center in the United States first proposed the concept of XCOM and conducted a communication verification experiment [1]. X-rays have a frequency range from 3×10^{16} Hz to 3×10^{19} Hz [2], which provides them with good directionality and penetration, and is higher than that for other carriers currently used for communication. High-energy X-rays (with energy above 10 keV) can be transmitted without attenuation in the space environment [3] and have extremely high penetration even in the upper atmosphere of the earth and the plasma sheath for re-entry vehicle [4–6]. Therefore, XCOM has excellent potential in space and blackout communication.

In the XCOM system, the modulated X-ray source acts as the transmitter, and its performance directly determines the data rate of the system. Therefore, the modulated X-ray source should have the characteristics of high modulation bandwidth to support high communication rate, large tube current to gain high X-ray intensity, and low cut-off voltage for convenient control. The present modulated X-ray sources mainly include light-controlled modulated X-ray tube (LMXT) [7–9]

and grid-controlled modulated X-ray tube (GMXT) [10–12], which control the X-ray intensity by adjusting the characteristics of the light source and grid voltage, respectively. Ma et al. [12] designed a GMXT with a cut-off voltage of −10 V@20 kV and tested the X-ray pulse of 10 kHz. Sheng et al. [3] transmitted voice signals by GMXT with a cut-off voltage of −1.6 V@10 kV at communication rate of 64 kbps. The pulse emission frequency of the LMXT developed by G.A. Timofeev et al. can reach 800 kHz [9]. Xuan et al. [13] developed a LMXT with 460 nm LED as the light source, the X-ray pulse emission frequency is 100 kHz, and the maximum tube current is 2.37 mA. In addition, field-emission X-ray tubes are also used to generate X-ray pulses [14–16].

The communication rate of the XCOM system with GMXT is determined by the performance of the grid voltage control circuit and the X-ray intensity [13]. If the cut-off voltage of GMXT is extremely large, then the modulation rate is low due to the bandwidth limitation of the grid voltage control circuit. The current commercial grid-controlled X-ray tubes have a cut-off voltage of several hundred to thousand volts and the pulse frequency of several tens of kHz, so they are not suitable for XCOM. Besides, GMXT with a small cut-off voltage [11], although a high-bandwidth control circuit can be used, often faces the problem

---

* Corresponding author at: Department of Nuclear Science and Technology, Nanjing University of Aeronautics and Astronautics, Nanjing 210016, China.
** Corresponding author.
E-mail addresses: liuyp@nuaa.edu.cn (Y. Liu), tangxiaobin@nuaa.edu.cn (X. Tang).

(a)

(b)
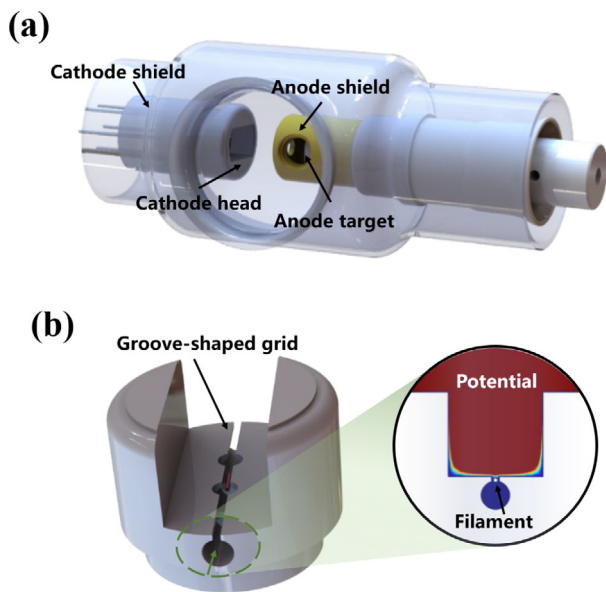
Fig. 1. (a) Overall structure of GGMXT, (b) groove-shaped grid structure.

Fig. 2. The structural parameters of the grid structure.

of insufficient X-ray intensity. It will reduce the signal-to-noise ratio of the X-ray signal. Therefore, reducing the cut-off voltage of GMXT and increasing the X-ray intensity are the primary tasks in the current research of GMXT. Given that X-rays have a continuous spectrum, the anode voltage must be higher than 10 kV to produce a sufficient number of effective photons over 10 keV. For blackout XCOM, Zhou et al. modeled the communication link and calculated that when the minimum power consumption is obtained, the anode voltage should be 50 kV [17]. However, the currently used GMXTs are designed with a preset anode voltage less than 30 kV. When their anode voltage is increased, their cut-off voltage also increases sharply and might reach tens of volts, leading to a low modulation rate during communication.

To solve the above problems, this work proposed the design of groove-shaped grid-controlled modulation X-ray tube (GGMXT). Under an increased preset anode voltage, a multi-objective optimization algorithm is used to improve the structure of its core component—the grid. This strategy aims to reduce the cut-off voltage and increase the X-ray intensity to provide XCOM with a reliable and high-performance transmitter.

2. Simulation and optimization of GGMXT

2.1. Description of the simulation model

Fig. 1 shows the structural schematic of GGMXT, consisting mainly of a reflective anode target, an anode shield, a cathode head, a cathode shield, and a thermal cathode filament. On the basis of the cathode head of the traditional X-ray diode, a groove-shaped grid is added to control the intensity of the electron beam emitted from the filament inside. The potential and electric field distribution near the filament can be changed by adjusting the voltage loaded on the grid. Therefore, the intensity of the electron beam passing through the opening of the groove can be controlled. The distance between the filament and the grid opening is only a few millimeters, and a small voltage is applied to the grid to cut off the emitted hot electrons almost instantaneously, so that GGMXT has a very fast modulation rate and a small grid control voltage. The grid and cathode head refer to the same component later in this paper.

The CST particle studio can be used to calculate the interaction between charged particles and electromagnetic fields. In this work, the simulation model of GGMXT is established by CST. In the thermionic emission mode, the temperature of tungsten filament is 2600 K, the anode voltage is 50 kV, and the initial grid voltage is 0 V.
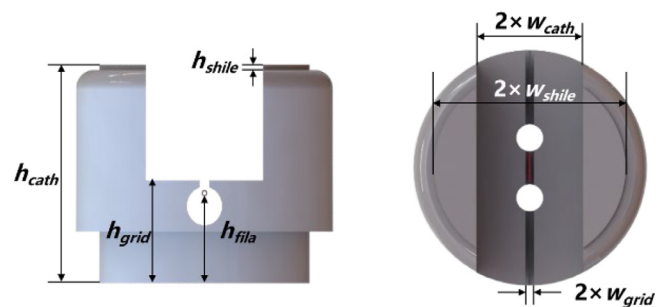
2.2. Screening of structural parameters for optimization

The modulation performance parameters of GGMXT mainly include cut-off voltage (U_{cut}), time dispersion (T), and tube current (I). N_e is the number of electrons bombarding the anode when the grid voltage is 0 V, and its value is proportional to the tube current and the X-ray intensity. Therefore, Ne is used to approximate the tube current in the simulation. U_{cut} is the grid voltage when the electron beam is wholly cut off and determines the complexity of the transmitter control circuit. Owing to the uneven distribution of the electric field and initial position, the dispersion of the arrival time of cathode electrons to the anode is called time dispersion (T), one of the primary limits of the communication rate.

Parameter pre-screening was first conducted to understand the influence of the relevant parameters of grid structure on the performance of GGMXT and select the key parameters. Fig. 2 shows the structural parameters for screening.

Part of the calculation results are shown in Fig. 3. The changes on the structural parameters affect the time dispersion of electrons at the nanosecond scale. Given that the data rate of XCOM has not reached Mbps, the influence of time dispersion caused by structure can be ignored. For most of the grid parameters, the changes of them greatly affect the modulation performance of GGMXT. This finding is in agreement with the results in Figs. 3(a) and 3(b). N_e and U_{cut} show approximately the same change trend with the changing in the grid structure parameters. Increasing N_e while reducing U_{cut} is a problem faced during the optimization. By contrast, Figs. 3(c) and 3(d) reflect that the changes in h_{shile} and w_{shile} have minimal effect on the performance of GGMXT. Therefore, only the five structural parameters of h_{cath}, h_{grid}, h_{fila}, w_{cath}, and w_{grid} are considered in the structural optimization. The optimization of the grid structure is a complex multi-objective optimization problem.

2.3. Structure optimization of GGMXT

2.3.1. Principle of NSGA-II

Non-dominated sorting genetic algorithm II (NSGA-II) is a multi-objective genetic algorithm that is based on non-dominated sorting [18, 19] and reduces computational complexity by introducing fast non-dominated sorting algorithms, elite strategies, and crowding distances. This algorithm does not need to assign weights to multiple objectives separately. Individuals in the Pareto front can evenly expand to the entire Pareto domain the diversity of the population. The basic idea of the NSGA-II algorithm is as follows:

(1) Generate an initial population P_t with a scale of N through random simulation, create an offspring population Q_t, and combine the above two populations to form a population R_t with a scale of $2N$;
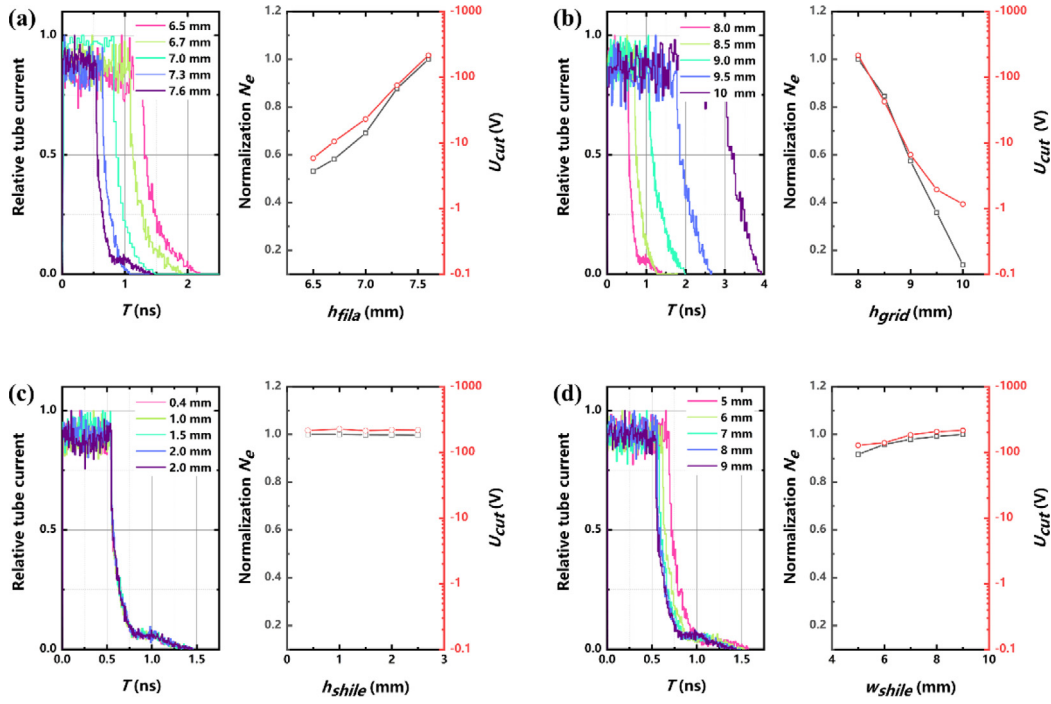
Fig. 3. Influence of (a) h_{grid}, (b) h_{fila}, (c) h_{shile}, and (d) w_{shile} on modulation performance. The picture on the left represents time dispersion (T), and the right one shows anode electron (N_e) and cut-off voltage (U_{cut}).

(2) Conduct fast non-dominated sorting on R_t. Calculate the crowding distances of the individuals in each non-dominated layer. Select appropriate individuals according to the non-dominated relationship and the crowdedness of the individuals to form a new parent population P_{t+1};

(3) Generate a new offspring population Q_{t+1} through genetic operation. Merge P_{t+1} and Q_{t+1} to form a new population, R_{t+1}. Repeat the above operation until the end conditions are met.

2.3.2. Algorithm realization

The optimization is realized through CST-Matlab co-simulation. CST is used as the objective function, and the main body of the NSGA-II algorithm is executed in Matlab. Fig. 4 shows the flow chart of the optimization process.

The objective functions have two objectives: (O1) the number of anode electrons and (O2) cut-off voltage. Their values are all calculated by CST. In the CST model, the number of electrons reaching the anode (N_a) is recorded when $V_g = 0$, and then $N_e = N_a$. U_{cut} is calculated using the binary search method. The boundary of V_g is specified as [V_l, V_h], $V_g = (V_l + V_h)/2$, the value of V_g in the model is modified, and N_a is calculated when $N_a = 0$ and $U_{cut} = V_g$.

During the optimization, a population consists of 40 binary-coded chromosomal structures, and the number of genetic iterations is set to 50. One chromosome structure represents one structural combination of GGMXT: $obj(U_{cut}, N_e) = obj(h_{cath}, h_{grid}, h_{fila}, w_{cath}, w_{grid})$.

2.3.3. Optimization results

The Pareto front recorded during 50 genetic iterations in Fig. 5 shows that the NSGA-II algorithm converges well for this optimization problem. When the genetic iteration reaches the 50th generation, it exhibits a uniform Pareto front. According to the optimization results, except for extreme solution, the minimum U_{cut} is −0.3 V, and the maximum U_{cut} is −71 V at anode voltage of 50 kV. Their corresponding N_e values are 54.8% and 99.0% of the maximum value, respectively. The optimization solutions on the Pareto front have their own advantages in different objectives, and the appropriate solution can be selected according to the actual requirements.
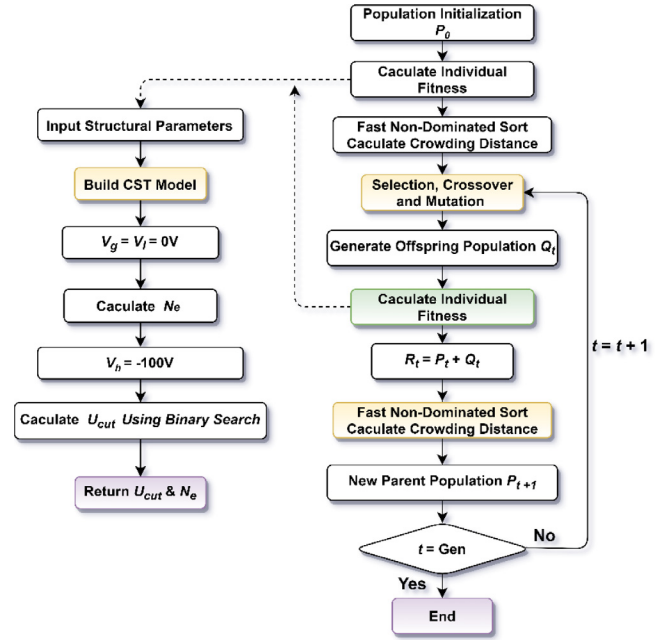

Fig. 4. Algorithm realization of grid structure optimization.

3. GGMXT prototype test

3.1. Introduction of GGMXT prototype

Three GGMXT prototypes selected from the Pareto solution set were prepared to verify the effectiveness of the optimization method. There were obvious differences in the two optimization objectives of these prototypes. As shown in Fig. 6, the optimized grid structure were adopted by Opt. 1 ($h_{grid} = 2.07$ mm, $h_{fila} = 6.84$ mm), Opt. 2 ($h_{grid} = 6.70$ mm, $h_{fila} = 7.15$ mm), and Opt. 3 ($h_{grid} = 5.86$ mm,
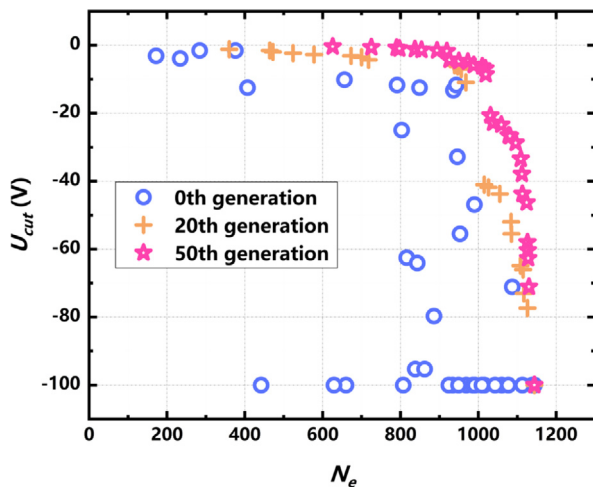
Fig. 5. Distribution of objectives: N_e (O1) and U_{cut} (O2).

Table 1
Comparison of measurement and simulation results.

	Experimental result		Simulation result	
	U_{cut} (V)	Relative N_e	U_{cut} (V)	Relative N_e
Opt. 1	−4.91	1.159	−4.88	1.418
Opt. 2	−23.43	1.517	−24.71	1.598
Opt. 3	−63.87	1.620	−62.70	1.644
Non. 1	−64.64	1	−62.70	1

h_{fila} = 7.34 mm). Non. 1 (h_{grid} = 0.4 mm, h_{fila} = 7.75 mm) was the non-optimized tube whose structural parameters were based on empirical values. This article focuses on the optimization of the grid structure, so there is no discussion on the selection of the cathode. The filament solenoids were the most common metal tungsten hot cathode, and anode targets were also made of metal tungsten. The vacuum chambers were made of glass. X-rays were emitted from the beryllium window on the side of the glass chamber. The production error of the grid assembly was ±0.1 mm.

3.2. I–V characteristic test

Fig. 7(a) shows the measurement of the X-ray intensity-grid voltage (I–V) characteristic of GGMXT prototypes. In order to meet the heat dissipation and insulation requirements of the tube, the tube was immersed in insulating oil in the experiment. After the amplification by the grid voltage control circuit, a constant voltage signal was loaded on the grid of GGMXT. At 10 cm from the beryllium window, an X-ray dose rate meter was used to measure the dose rate value in order to characterize the X-ray intensity. During the measurement, the filament current was set to 1.2 A, and the anode voltage was set to 50 kV. The grid voltage is directly measured by a multimeter with an accuracy of 0.01 V. The results are shown in Fig. 7(b). When the grid voltage is 0, the X-ray emission intensity of Opt. 1 and Opt. 2 are increased by 15.9% and 51.7% respectively, and their U_{cut} values are greatly reduced compared with those of Non. 1. The U_{cut} of Opt. 3 is the same as that of Non. 1, but its X-ray intensity is improved by 62.0%.

Table 1 shows the comparison of measurement and simulation results. The experimental cut-off voltage is similar to the simulation results with the relative error of less than 5.3%. The relative X-ray intensity of Opt. 1 is lower than the expected value, and those of Opt. 2, Opt. 3 and Non. 1 are almost same as the simulations. In consideration of the structural errors during the production of GGMXT and their consequent influences on the X-ray intensity, the experimental data are in agreement with the simulations within the error range. These results indicate that CST-Matlab co-simulation based on the NSGA-II algorithm is a good optimization method for modulated X-ray tubes.

3.3. Tube current characteristic test

The filament current determines the number of thermionic electrons produced by the cathode for the hot cathode X-ray tube [20]. The anode voltage determines the proportion of thermionic electrons drawn to the anode and converted into X-ray photons, which determine the tube current. Fig. 8 shows the relationship among filament current, anode

voltage, and tube current of the three optimized structures Opt. 1, Opt. 2, and Opt. 3. The tube current is directly collected by the feedback circuit of the high-voltage power supply.

When the filament current is small, the tube current of three tubes are similar, and the tube current increases slowly with the anode voltage until saturation is reached. With the increase in filament current and anode voltage, the change trend of tube current shows a big difference. The higher the cut-off voltage of the tube, the more intense the increase in tube current. This is because the grid structure with a small cut-off voltage has a strong shielding effect on the anode electric field. Although the increase in filament current leads to a sharp increase in the number of generated hot electrons, the excellent shielding effect of grid makes hot electrons cannot reach the anode. Hence, the tube current always maintains a lower level.

3.4. Frequency response test

The modulation performance of GGMXT was tested on the XCOM test platform which is shown in Fig. 9. A signal generator was used to produce the initial modulation signal, which was then amplified by the grid voltage control circuit and loaded on the grid to control the intensity of the electron beam in GGMXT. The X-ray signal containing the modulation information was subsequently generated. At the detection end, a LYSO-SiPM detector [21] was used to convert the X-ray intensity signal into an electrical signal through the photoelectric effect. Finally, the electrical signal was processed by a high-speed data acquisition card.

Fig. 10 shows the frequency response of GGMXT. During the measurement, the amplitude of the sinusoidal signal with DC offset output by the grid voltage control circuit was kept at a constant value, and the amplitude of the detected X-ray signal was measured. The filament current was 1.2 A, and the anode voltage was 50 kV. The bandwidth of GGMXT Opt. 1, Opt. 2, and Opt. 3 are above 3 MHz, and the frequency response curves of the three have high consistency. However, this does not mean that the difference in structural parameters has no effect on the bandwidth of the tube, because the detector output waveform is the convolution of the X-ray signal and the detector impulse response which is 300–500 ns. This will result in attenuation of signal amplitude when measuring sinusoidal signals higher than about 2 MHz. The test results for the frequency response are mainly limited by the bandwidth of the detector and thus cannot reflect the actual performance of GGMXT. Therefore, these experimental results are only used as a reference for the performance of GGMXT, and the actual bandwidth should be higher than them. Nevertheless, the bandwidth of 3 MHz is still the highest among current grid-controlled and even optically modulated X-ray sources.

3.5. Pulse emission test

Currently, pulse modulation is commonly used in XCOM. The original signal was changed to a square wave, and the pulse X-ray emission performance of GGMXT was tested on the test platform described in the previous section. A square wave signal with an amplitude of −5 V and a duty cycle of 50% was loaded on the grid of Opt. 1, and the detected X-ray pulse waveform is shown in Fig. 11. The width of the rising edge of the detected square wave signal is about 80 ns, which
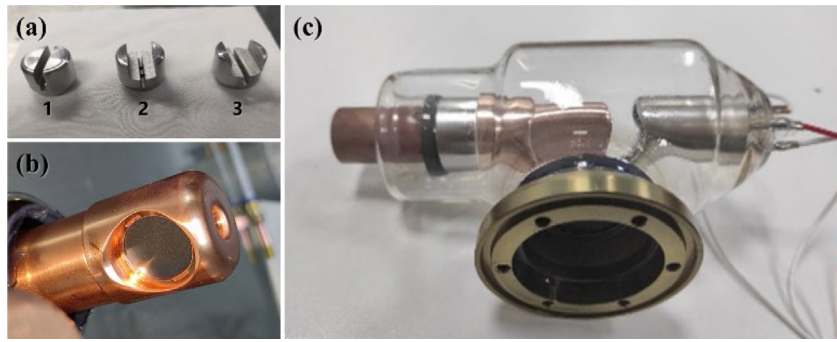
Fig. 6. (a) Optimized grid components, (b) anode component, and (c) GGMXT prototype.
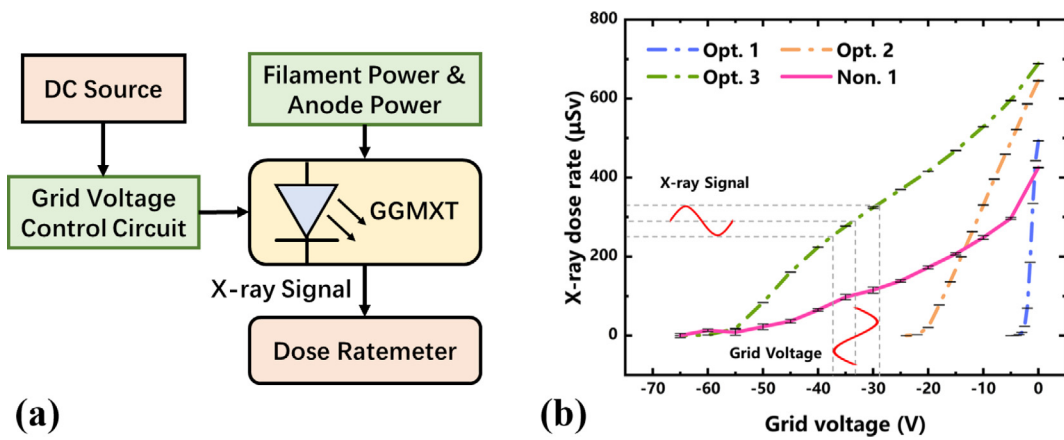

Fig. 7. (a) Schematic of the measurement of *I–V* characteristics. (b) *I–V* characteristics of GGMXT.
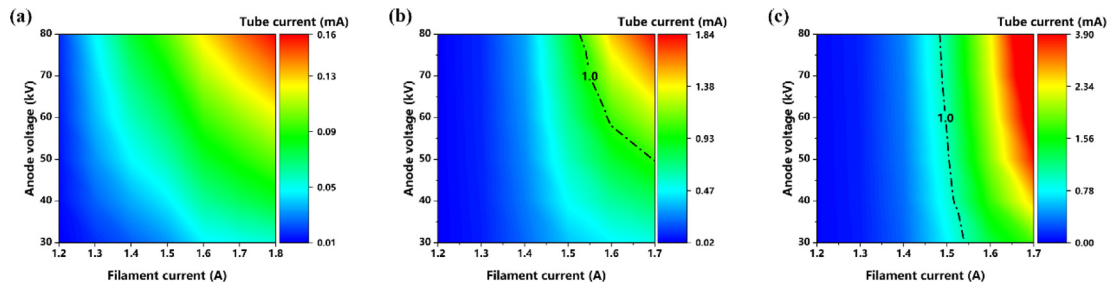

Fig. 8. Tube current characteristics of GGMXT: (a) Opt. 1, (b) Opt. 2. and (c) Opt. 3.
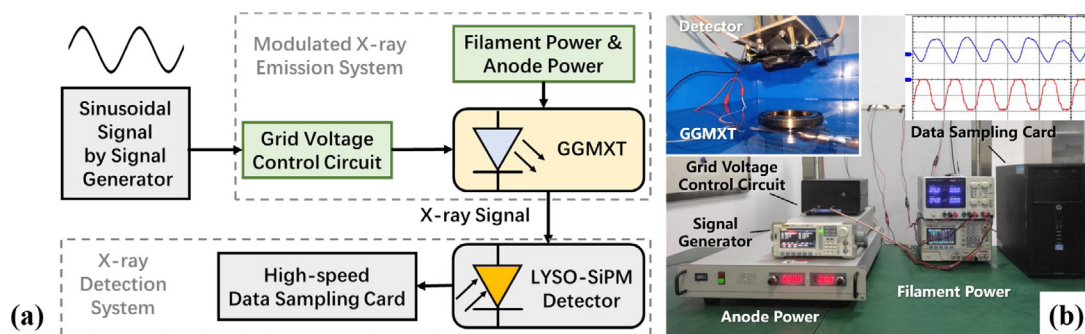

Fig. 9. (a) Schematic of the measurement of frequency response. (b) X-ray communication test platform.
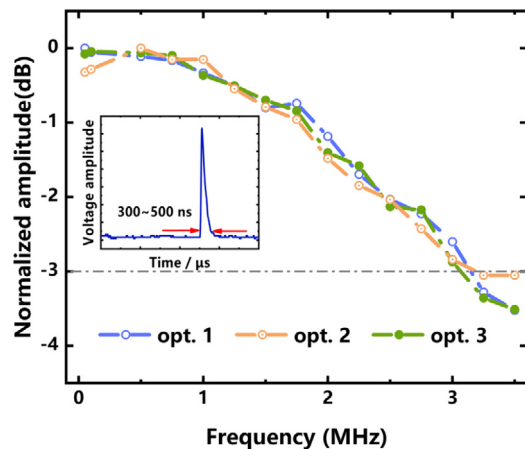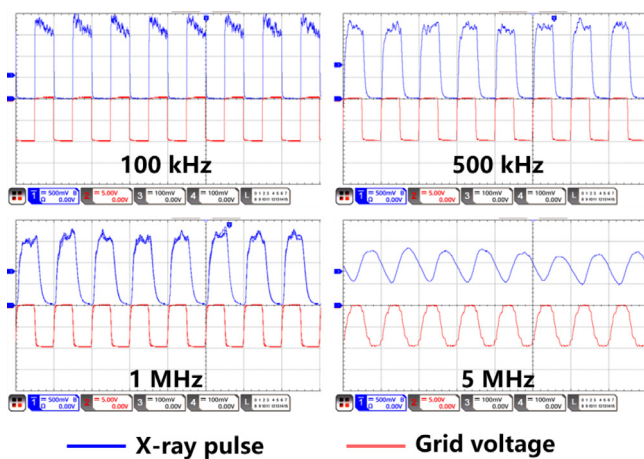
Fig. 10. Frequency response of GGMXT.

Fig. 11. The waveform of X-ray pulse and grid voltage.

is similar to the impulse response test result of the detector. The test results show that the excellent performance of GGMXT allows the X-ray pulse repetition rate in excess of several MHz.

In addition, the tube current (I_s) at different frequencies was also measured, which represents the number of electron charges reaching the anode per unit time. The measurement results show that the tube currents at different frequencies are very similar. When the waveform duty cycle is 50% and the filament current is 1.2 A and 1.7 A, the measured I_s is 0.008 mA and 0.04 mA respectively, which are approximately equal to half of the tube current in the continuous emission mode.

4. Conclusion

NSGA-II algorithm was used to optimize the design of the proposed GGMXT grid structure and provide it with the characteristics of low cut-off voltage and high emission X-ray intensity. The prototypes were prepared, and the effectiveness of the optimization method was verified through experimental measurement. The modulation bandwidth of prototypes in excess of 3 MHz is the highest level obtained among current grid-controlled modulation X-ray sources.

For the optimized GGMXT, the smaller the cut-off voltage, the smaller the corresponding tube current. In practical applications, it is necessary to comprehensively consider the requirements for tube current and cut-off voltage, and select the most appropriate design scheme. Furthermore, a hot cathode with better emission characteristics can be selected to increase the tube current. This work provides a

reference design for high-speed modulated X-ray sources and presents feasible transmitter for XCOM. For long-distance space XCOM, multiple transmitters can be combined into a synchronous transmission array, combined with X-ray focusing optical elements to increase the intensity of X-ray signals. In addition, GGMXT can also provide more options for high-speed X-ray imaging.

CRediT authorship contribution statement

Zhaopeng Feng: Methodology, Software, Data curation, Formal analysis, Visualization, Writing – original draft. **Yunpeng Liu:** Conceptualization, Methodology, Supervision, Writing – reviewing and editing. **Junxu Mu:** Writing – reviewing and editing. **Wenxuan Chen:** Writing – reviewing and editing. **Sheng Lai:** Writing – reviewing and editing. **Xiaobin Tang:** Supervision, Project administration, Writing – reviewing and editing.

Declaration of competing interest

The authors declare that they have no known competing financial interests or personal relationships that could have appeared to influence the work reported in this paper.

Acknowledgment

References

[1] National Aeronautics and Space Administration, NASA technology roadmaps TA 5: Communications, navigation, and orbital debris tracking and characterization systems, 2015, NASA Technol. Roadmaps.

[2] S.J. Edwards, X-ray wavelength units, Phys. Educ. 5 (1970) 82–84, http://dx.doi.org/10.1088/0031-9120/5/2/001.

[3] L. Sheng, B. Zhao, Y. Liu, Novel space communication technology based on modulated x-ray source, in: Adv. X-Ray/EUV Opt. Components IX, SPIE, 2014, 920716, http://dx.doi.org/10.1117/12.2062712.

[4] Y. Liu, H. Li, Y. Li, S. Hang, X. Tang, Transmission properties and physical mechanisms of X-ray communication for blackout mitigation during spacecraft reentry, Phys. Plasmas 24 (2017) http://dx.doi.org/10.1063/1.4998786.

[5] H. Li, X. Tang, S. Hang, Y. Liu, D. Chen, Potential application of X-ray communication through a plasma sheath encountered during spacecraft reentry into earth's atmosphere, J. Appl. Phys. 121 (2017) 123101, http://dx.doi.org/10.1063/1.4978758.

[6] Y. Li, T. Su, L. Sheng, N. Xu, B. Zhao, Simulation and experiment of X-ray communication in re-entry dusty plasma region, Modern Phys. Lett. B 34 (2020) 1–13, http://dx.doi.org/10.1142/S0217984920500578.

[7] S. Sproch, S. Strohkorb, C. Frankenfeld, J. Bethune, Digital X-ray signal transmission, 2011, pp. 1–12.

[8] S. Hang, Y. Liu, H. Li, X. Tang, D. Chen, Temporal characteristic analysis of laser-modulated pulsed X-ray source for space X-ray communication, Nucl. Instrum. Methods Phys. Res. A 887 (2018) 18–26, http://dx.doi.org/10.1016/j.nima.2018.01.031.

[9] G.A. Timofeev, N.N. Potrakhov, A.I. Nechaev, Experimental research of the x-ray communication system, AIP Conf. Proc. 2089 (2019) 2–7, http://dx.doi.org/10.1063/1.5095749.

[10] F. Zhou, G.M. Wu, B.S. Zhao, L.Z. Sheng, J. Song, Y.A. Liu, Q.R. Yan, N.Q. Deng, J.J. Zhao, An analog modulated simulation source for X-ray pulsar-based navigation, Wuli Xuebao/Acta Phys. Sin. 62 (2013) http://dx.doi.org/10.7498/aps.62.119701.

[11] H. Mou, B.Q. Li, Y. Cao, Transmission-type miniature micro-beam modulated X-ray source based on space application, Wuli Xuebao/Acta Phys. Sin. 65 (2016) http://dx.doi.org/10.7498/aps.65.140703.

[12] X.F. Ma, B.S. Zhao, L.Z. Sheng, Y.A. Liu, D. Liu, N.Q. Deng, Grid-controlled emission source for space X-ray communication, Wuli Xuebao/Acta Phys. Sin. 63 (2014) http://dx.doi.org/10.7498/aps.63.160701.

[13] H. Xuan, Y.-A. Liu, P.-F. Qiang, T. Su, X.-H. Yang, L.-Z. Sheng, B.-S. Zhao, Light-controlled pulsed X-ray tube with photocathode, Chin. Phys. B (2021) http://dx.doi.org/10.1088/1674-1056/abff1e.

[14] G.Z. Yue, Q. Qiu, B. Gao, Y. Cheng, J. Zhang, H. Shimoda, S. Chang, J.P. Lu, O. Zhou, Generation of continuous and pulsed diagnostic imaging x-ray radiation using a carbon-nanotube-based field-emission cathode, Appl. Phys. Lett. 81 (2002) 355–357, http://dx.doi.org/10.1063/1.1492305.

[15] J.T. Kang, H.R. Lee, J.W. Jeong, J.W. Kim, S. Park, M.S. Shin, J.H. Yeon, H. Jeon, S.H. Kim, Y.C. Choi, Y.H. Song, Fast and stable operation of carbon nanotube field-emission X-ray tubes achieved using an advanced active-current control, IEEE Electron Device Lett. 36 (2015) 1209–1211, http://dx.doi.org/10.1109/LED.2015.2478157.

[16] S. Lai, X. Tang, Y. Liu, J. Mu, Z. Feng, K. Miao, X-ray high frequency pulse emission characteristic and application of CNT cold cathode x-ray source cathode x-ray source, Nanotechnology 33 (2021) http://dx.doi.org/10.1088/1361-6528/ac378b.

[17] W. Zhou, X. Tang, Y. Liu, S. Hang, H. Li, J. Mu, P. Dang, S. Lai, Power budget and performance analysis of X-ray communication during the Earth re-entry of spacecraft, Optik (Stuttg) 199 (2019) 163521, http://dx.doi.org/10.1016/j.ijleo.2019.163521.

[18] A. Seshadri, A fast elitist multiobjective genetic algorithm: NSGA-II, Mathlab Central, file exchange, mathworks, 2007, pp. 1–4.

[19] S.W. Cheng, H. Zhang, L.C. Shen, J. Tian, Optimization of regional coverage reconnaissance satellite constellation by GDE3 algorithm, Xitong Fangzhen Xuebao/ J. Syst. Simul. 21 (2009) 586–589.

[20] A. Ihsan, S.H. Heo, S.O. Cho, Optimization of X-ray target parameters for a high-brightness microfocus X-ray tube, Nucl. Instrum. Methods Phys. Res. B 264 (2007) 371–377, http://dx.doi.org/10.1016/j.nimb.2007.09.023.

[21] Y. Liu, P. Dang, X. Tang, J. Mu, Z. Feng, Performance analysis of LYSO-SiPM detection module for X-ray communication during spacecraft reentry blackout, Nucl. Inst. Methods Phys. Res. A (2021) 165673, http://dx.doi.org/10.1016/j.nima.2021.165673.